ACS APPLIED MATERIALS & INTERFACES

Research Article

www.acsami.org

# Ultrafast Carrier Dynamics and Hot Electron Extraction in Tetrapod-Shaped CdSe Nanocrystals

Pengtao Jing,[†] Wenyu Ji,*[,†] Xi Yuan,[‡] Songnan Qu,[†] Renguo Xie,[§] Michio Ikezawa,[∥] Jialong Zhao,*[,‡] Haibo Li,[‡] and Yasuaki Masumoto[∥]

[†]State Key Laboratory of Luminescence and Applications, Changchun Institute of Optics, Fine Mechanics and Physics, Chinese Academy of Sciences, 3888 Eastern South Lake Road, Changchun 130033, China

[‡]Key Laboratory of Functional Materials Physics and Chemistry of the Ministry of Education, Jilin Normal University, Siping 136000, China

[§]College of Chemistry, Jilin University, Changchun 130012, China

[∥]Institute of Physics, University of Tsukuba, Tsukuba, Ibaraki 305-8571, Japan

Supporting Information

**ABSTRACT:** The ultrafast carrier dynamics and hot electron extraction in tetrapod-shaped CdSe nanocrystals was studied by femtosecond transient absorption (TA) spectroscopy. The carriers relaxation process from the higher electronic states ($CB_2$, $CB_{3(2)}$, and $CB_4$) to the lowest electronic state ($CB_1$) was demonstrated to have a time constant of 1.04 ps, resulting from the spatial electron transfer from arms to a core. The lowest electronic state in the central core exhibited a long decay time of 5.07 ns in agreement with the reported theoretical calculation. The state filling mechanism and Coulomb blockade effect in the CdSe tetrapod were clearly observed in the pump-fluence-dependent transient absorption spectra. Hot electrons were transferred from arm states into the electron acceptor molecules before relaxation into core states.

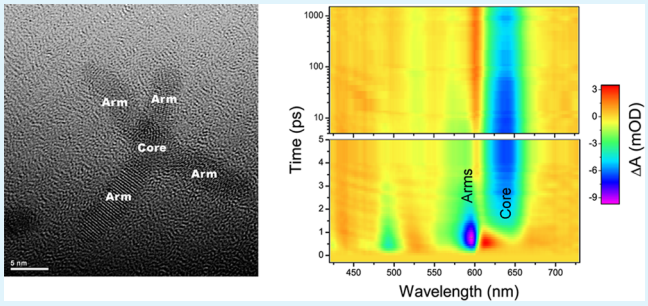


**KEYWORDS:** *tetrapod, nanocrystals, carrier dynamics, electron transfer, transient absorption spectroscopy*

## 1. INTRODUCTION

Progresses in the synthesis have enabled us to control accurately the shape of semiconductor nanocrystals (NCs), having spherical, linear, and branched structures.[1−6] Unlike the change in size, the change in shape can result in the change in electronic structure, including the state energy, the overall shape of the wave function, the symmetry, the polarization, and the localization of carriers.[7,8] Tetrapod is an electronically coupled semiconductor NC molecule with four arms branched from a central core at the tetrahedral angle.[8] The energy levels and the wave functions of electronic states in the tetrapod-shaped CdSe NC were calculated by a semiempirical pseudopotential method (SEPM).[7] The lowest electronic state (conduction band, $CB_1$) is localized in the central tetrahedron and the highest hole state (valence band, $VB_1$) is extended into the arms of the tetrapod.[7] In single tetrapod-shaped NC transistor, two arms were used as the two electrodes and another arm was used as the electric-field control gate.[9] Because of the localization of the electronic state, the electron transport properties of single-electron transistor based on CdSe tetrapods were dramatically controlled by the sensitive arm-gate.[7,9] Tetrapod-shaped NCs could be applied as optical strain gauge, because of their sensitive strain-dependent electronic level structure.[10,11] It has been demonstrated that tetrapod-shaped NCs lead to better solar cell performance than both nanorods and quantum dots, because of the improved electron transport perpendicular to the plane of the film, independent of the orientation of NCs.[12−15] Dual photoluminescence (PL) and electroluminescence (EL) emissions from multiple excited levels were observed in CdSe/CdS core/shell tetrapod, which violated Kasha's rule.[16,17] The electric-field-controlled exciton storage was observed in CdSe/CdS tetrapods and attributed to states filling of discrete trap state in CdS arms.[18] However, controlling carrier transport and localization via NC's morphology is still a challenge for scientists.

The femtosecond transient absorption (TA) spectroscopy based on the time-resolved pump−probe method is a powerful tool to investigate the ultrafast carrier dynamics in semiconductor NCs.[19−24] The state filling in the NCs leads to a negative bleaching signal of the interband optical transitions involving populated quantized states. For CdSe quantum dots, size dependent carrier relaxation process from high-energy states to low-energy states and state filling mechanism of 1S

Received: December 26, 2014
Accepted: April 2, 2015
Published: April 2, 2015





DOI: 10.1021/am5091148
ACS Appl. Mater. Interfaces 2015, 7, 7938−7944

and 1P states were observed in pump-dependent TA spectra. On the other hand, Coulomb interaction induced Auger recombination was quantitatively analyzed by varying the average electron−hole pairs per NC and size of NC. the ultrafast carrier dynamics determines the optical and electrical properties of semiconductor quantum dots or tetrapod-shaped NC.[23] The electron−hole dynamics of CdTe tetrapods and the localization of the excited-state wave functions were studied by the TA spectroscopy.[19] Charge separation was induced by type II alignment in CdSe/CdTe tetrapod heterostructures.[20] Mauser et al. studied the spatiotemporal electron−hole transfer and Coulomb drag in CdSe/CdS tetrapods by femtosecond time-resolved pump−probe and PL spectroscopy.[21] Up to now, there remains a fundamental question how the morphology-dependent electron states control the dynamics of the photogenerated carriers in NCs.

In this work, we studied the ultrafast electron transfer from the arms to the core in CdSe tetrapod-shaped NCs by femtosecond TA spectroscopy. The state filling mechanism in the tetrapod was discussed by measuring the pump-fluence-dependent spectroscopy. Ultrafast charge separation from tetrapods to organic electron acceptors was also studied to understand the extraction of hot electrons.

## 2. EXPERIMENTAL SECTION

**Synthesis of Tetrapod-Shaped CdSe Nanocrystals (NCs) and Optical Characterization.** CdSe tetrapods were synthesized following ref 6. UV−vis absorption and PL spectra were taken with a UV−vis−NIR scanning spectrophotometer (Shimadzu, UV-3101PC) and a spectrophotometer (Hitachi, F-7000), respectively.

**Preparation of $MB^+$-Tetrapod Complex.** $MB^+$ (methylene blue hydrate, purity ≥97.0%) was purchased from Aldrich without further purification. $MB^+$ molecules (5 μL, 2 mg/mL dispersed in methanol) were added into NC solution (3.5 mg/mL, 200 μL in quartz cuvettes with optical path of 1 mm) and ultrasonic dispersion 10 min.

**Transient Absorption (TA) Spectroscopy.** Ultrafast TA experiments were conducted using a Ti:sapphire laser (Spectra-Physics, 800 nm, 0.3 mJ/pulse, fwhm 120 fs, 1 kHz repetition rate). The white-light probe was generated by the fundamental laser output focused on a CaF2 window with 5 mm thickness. The probe beam at the sample had a diameter of 150 μm. Pump pulses at 400 nm were generated by frequency doubling of the fundamental laser in a BBO crystal. The pump beam at the sample had a diameter of 660 μm. The energy pump beam used for the measurement was controlled by a variable neutral-density filter wheel. The energy of the pump pulse was changed by a variable neutral density filter. The pump pulses were chopped by a synchronized chopper to 500 Hz. After passing through the sample, the probe beam was focused into a fiber-coupled spectrometer (Avantes; AvaSpec-1650F-USB2,). The angle between pump and probe polarizations was set at magic angle (54.6°) to ensure the dynamics free from reorientation effects. The group velocity dispersion of the whole experimental system was compensated by a chirp program. During the data collection, samples were constantly stirred to avoid degradation. All experiments were performed at room temperature.

## 3. RESULTS AND DISCUSSION

The CdSe tetrapod-shaped NCs were synthesized by the method described in Xie's report.[6] The morphology of CdSe tetrapods was characterized by transmission electron microscopy (TEM), as shown in Figures 1 and S1 in Supporting Information. The arms of the tetrapod NCs were determined to have a length of 11 nm and a diameter of 3.5 nm; the diameter of the spherical core was 5 nm according to the TEM measurement. The tetrapod had $T_d$ symmetry, and it had a tetrahedron with zincblende (ZB) crystal structure at its center.[1] This central core was connected by four wurtzite (WZ) structure nanorods at the (111), $(\bar{1}\bar{1}1)$, $(1\bar{1}\bar{1})$, and $(\bar{1}1\bar{1})$ surfaces, as shown in the inset of Figure 1.[7] The arms of CdSe tetrapods NCs were pure wurtzite growth along *c* axis (WZ (0001) direction), as seen in Figure S1 in Supporting Information.

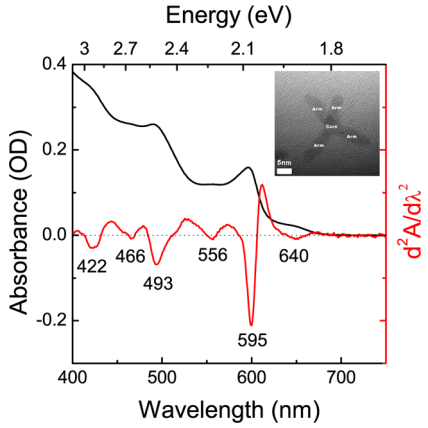


**Figure 1.** Steady-state absorption spectrum (black line) of tetrapod-shaped CdSe NCs. The second derivative of the broad absorption spectrum is shown by a red line. The inset shows TEM images of tetrapod-shaped CdSe NCs (denoted as core/arms) prepared by the seeded-growth approach.

In a previous report, it has been surprisingly found that the lowest conduction band $CB_1$ is completely localized in the central tetrahedron and the second, third, and fourth states ($CB_2$, $CB_{3(2)}$, and $CB_4$) are extended into the arms of the tetrapod.[7] The electronic state $CB_{3(2)}$ and the highest hole state of valence band $VB_{1(2)}$ are doubly degenerated.[7] The CdSe tetrapod modeled for the previous calculation was set up 2817 atoms, and the four arms of the nanorod were 2.2 nm in diameter and 4.6 nm in length. The energy difference between $CB_2$ ($CB_{3(2)}$) and $CB_{3(2)}$ ($CB_4$) was 2 (26) meV. However, the size of the modeled tetrapod is smaller than that of the CdSe tetrapod used in our experiment. Hence, the actual energy difference between $CB_2$, $CB_{3(2)}$, and $CB_4$ will be smaller in our sample used in the experiment. It can be assumed that these electronic states are nearly degenerated. Therefore, the transitions $VB_{1(2)} \rightarrow CB_2$, $VB_{1(2)} \rightarrow CB_{3(2)}$, and $VB_{1(2)} \rightarrow CB_4$ are difficult to decide from the overlapped spectrum, corresponding to the strong excitonic absorption peak around 595 nm, as seen in Figure 1.[22] The lowest excitonic absorption peak at wavelength of 640 nm is weak, which is attributed to the transition $VB_{1(2)} \rightarrow CB_1$.[10] The spectral positions of the excitonic absorption peaks (640, 595, 556, 493, 466, 422 nm) are clearly distinguished by the second derivative of the absorption spectrum as seen in Figure 1. The energy difference between the bands (595 and 556 nm) is about 146 meV, which is close to the calculated value (~130 meV) between $CB_{2,3(2),4}$ and $CB_{5,6(2)}$. Therefore, the absorption peak at 556 nm is attributed to the transition $VB_{1(2)} \rightarrow CB_{5,6(2)}$. Absorption peaks at 493, 466, and 422 nm are assigned to the higher electronic states.

To understand the electron−hole dynamics of the tetrapod-shaped CdSe NCs, the femtosecond TA spectroscopy in the visible spectral range was performed. Figure 2a shows the TA spectra measured at low pump fluence (13 $\mu J/cm^2$), avoiding multiple photon absorption of one NC.[23] The chirp-corrected TA spectra of CdSe Tetrapod NCs at different delay time are


DOI: 10.1021/am5091148
ACS Appl. Mater. Interfaces 2015, 7, 7938−7944

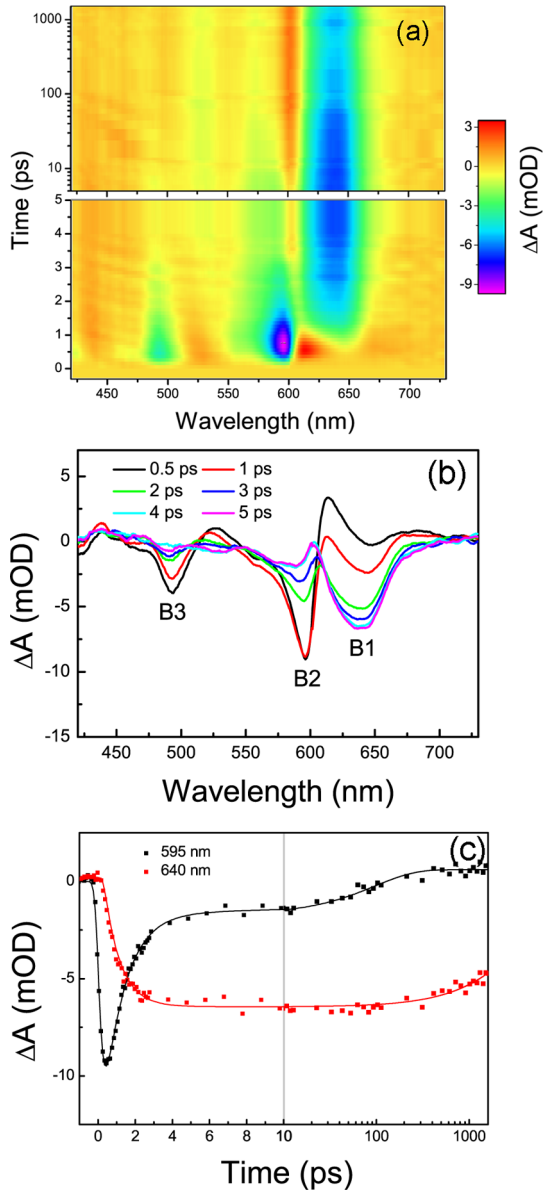


**Figure 2.** (a) TA changes (0−1600 ps) and (b) TA spectra of CdSe tetrapods at indicated delay times (0.5−5 ps) after excitation at $\lambda_{pump}$ = 400 nm (at lowest intensity, 13 $\mu J \cdot cm^{-2}$). B1 (640 nm), B2 (595 nm), and B3 (493 nm) are three bleach peaks in TA spectra. (c) Bleach signal kinetics of CdSe tetrapods. Probe wavelengths are 595 nm (black line) and 640 nm (red line), respectively.

shown in Figure 2b. There are three obvious bleaching peaks at 640, 595, and 493 nm labeled by B1, B2, and B3, respectively. The TA spectral feature is well consistent with the second derivative of the absorption spectrum. The photobleaching signals at 640 (B1) and 595 nm (B2) can be attributed to the electronic state filling of $CB_1$ and $CB_{2,3(2),4}$.[7,23,24] The energy difference between B1 and B2, 146 meV, is smaller than 178 meV of the calculated one between $CB_1$ and $CB_2$.[7] Peak B3 may result from state filling of the higher electronic state, so-called hot electron. Figure 2c shows the bleach signal kinetics of B1 and B2. The experimental data were fitted by single exponential rise and double exponential decay functions. The rise and decay time constants of B2 (595 nm) are determined to be 0.22 and 1.04 ps, respectively. The B2 peak reaches its maximum at 0.5 ps after the excitation while the B1 peak (640 nm) is still small at the same time, indicating that the electron first fills into $CB_{2,3(2),4}$ after pump excitation. The B2 peak decreases rapidly with increasing the delay time from 0.5 to 5 ps, but the B1 peak is gradually enhanced, as seen in Figure 2b. The buildup and decay time constants of B1 (640 nm) are fitted to be 0.86 ps and 5.07 ns, respectively. It is noted that the decay time constant of B3 (595 nm) is 0.99 ps, as show in Figure S3 in Supporting Information. The decay time constants of the B2 and B3 peak are close to the buildup time constant of the B1 peak, indicating the rapid relaxation of carriers from higher electronic states to the lowest electronic state. However, the maximum bleaching amplitudes of B1, B2, and B3 are about 7, 10, 4 mOD, which is related to the carrier populations at corresponding states. The carrier population at state B2 is more than that at state B3. On the other hand, there are surface trap sates and middle electronic states between B1 (640 nm) and B3 (493 nm), the relaxation from B3 to B1 is not the only depopulation path for B3. Therefore, carrier relaxation from $CB_{2,3(2),4}$ to $CB_1$ is the main contribution for buildup of bleaching peak B1 (640 nm). Because electronic wave functions of $CB_1$ and $CB_{2,3(2),4}$ are distributed at different areas of tetrapod,[7] the relaxation from $CB_{2,3(2),4}$ to $CB_1$ corresponds to the spatial electron transfer from arms to core. However, the electron cannot transfer from the long CdS arm to the CdSe core in CdSe/CdS core/shell tetrapod NC, due to the Coulomb drag of hole trap in the arms.[21] The lowest electronic state, $CB_1$, is localized in the core, which is far away from the surface defect states, thus the photobleaching signal at 640 nm has a long decay lifetime of more than 5 ns. The localization of the electronic state implies the device applications of the tetrapod.[7] Applying electric voltage on the control gate in tetrapod can drive the $CB_1$ state away from the tetrahedron center and then dramatically control the current in the conduction band.[9]

The pump fluence dependence of $\Delta A_{max}/A$ at wavelengths of 640 and 595 nm are shown in Figure 3a. $\Delta A_{max}$ is the maximum value of temporal absorption change after excitation, reflecting the state filling level at a given pump fluence. A ($A = \alpha d$) is the value of steady state absorption at the probed wavelength, limiting the saturation of the bleaching signal. With increasing the pump fluence, the maximum ΔA at 640 and 595 nm are close to the intensity of the steady state absorption peaks, corresponding to the complete bleaching of the transitions, as seen in Supporting Information Figure S2. When the pump fluence reaches 0.1 and 0.3 mJ/cm$^2$, the bleaching signals at 640 and 595 nm are close to saturation, respectively. The average number of photons absorbed per NC can be calculated using the expression[25−27]

$$\langle N_0 \rangle = J(0)\frac{1 - \exp(-\mathrm{OD} \times \ln 10)}{cL} \quad (1)$$

Here, $J(0)$ is the photon fluence of pump beam (presented in photons per cm$^2$), OD is the optical density at the excitation wavelength, $c$ is the concentration of the NC, and $L$ is the optical path length of the cuvette. In our experiment, the photon energy of the pump beam is greater than the energy gap of NCs, thus the probability for a NC to absorb N photons is independent of the number of e−h pairs already created in the NC and can be described by the Poisson distribution:[23,25,27]

$$P(N) = \langle N_0 \rangle^N e^{-\langle N_0 \rangle}/N! \quad (2)$$


DOI: 10.1021/am5091148
ACS Appl. Mater. Interfaces 2015, 7, 7938−7944

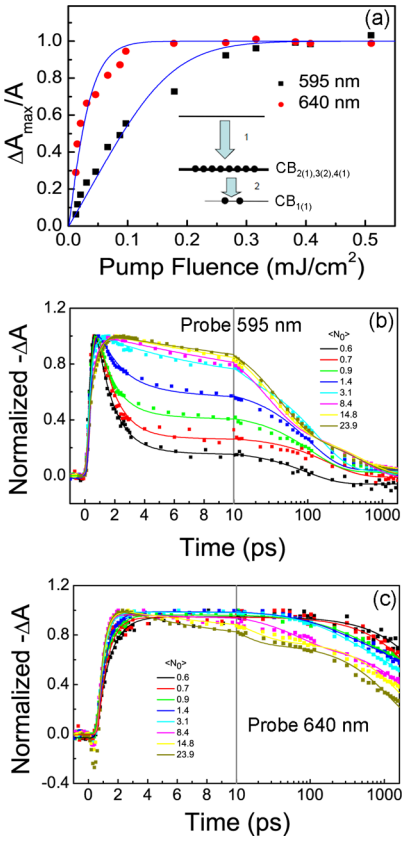


**Figure 3.** (a) Pump fluence dependence of the normalized bleaching signals at $\lambda_{probe}$ = 595 (black squares) and 640 nm (red cycles). Fitted lines (blue lines) are assumed by a Poisson type population growth function. Inset: After excitation, the hot electron at the high energy state first relaxes into the arm states $CB_{2(1),3(2),4(1)}$ and then relaxes into core state $CB_{1(1)}$. The numbers in parentheses represent the degeneracy. (b) Normalized bleach signal kinetics of B2 (595 nm) under different pump fluences. (c) Normalized bleach signal kinetics of B1 (640 nm) under different pump fluences. $\langle N_0 \rangle$ is the average number of photons absorbed by a tetrapod.

Here, $P(N)$ is the probability of NC to have $N$ e−h pairs if the average number of the photons absorbed per NC is $\langle N_0 \rangle$. After excitation, the hot electron at the high energy state first relaxes into the arm states $CB_{2,3(2),4}$, and then relaxes into core state $CB_1$, as shown in the inset of Figure 3a. The occupation numbers of the $CB_1$ and $CB_{2,3(2),4}$ states in this model can be calculated as follows:[27]

$$n^e_{CB1} = 0.5P(1) + \sum_{i=2}^{\infty} P(i) \quad (3)$$

$$n^e_{CB2,3,4} = \sum_{i=1}^{7} P(i) \times i/8 + \sum_{i=8}^{\infty} P(i) \quad (4)$$

Because $\langle N_0 \rangle$ is proportional to $J(0)$, the pump fluence dependence of the normalized bleaching signals at 640 and 595 nm can be fitted by eqs 3 and 4, as seen in Figure 3a. The calculated molar extinction coefficients at 400 nm are $9.6 \times 10^9$ and $9.2 \times 10^9$ $M^{-1}cm^{-1}$ for the fitted results at 640 and 595 nm, respectively. The molar extinction coefficient at 400 nm estimated from the TEM image and sample mass is $9.1 \times 10^9$ $M^{-1}$ $cm^{-1}$, which is close to the fitted ones. This indicates the assumption of near degenerated electronic states $CB_2$, $CB_{3(2)}$, and $CB_4$ is reasonable.

At the low pump fluence, the fast decay component at 595 nm is attributed to the relaxation from the arm states $CB_{2,3(2),4}$ to the core state $CB_1$. $\langle N_0 \rangle$ can be obtained by eq 1 as shown in Figure 3b and c. The decay curves are fitted by a multiexponential function with a raise component and two decay components. The fitted lifetimes of the arm states $CB_{2,3(2),4}$ are summarized in Table S1 in Supporting Information. With increasing the pump fluence, the decay lifetimes of $CB_{2,3(2),4}$ are enhanced from 1.04 to 40.15 ps, as seen in Figure 3b. If the $CB_1$ state is filled with one electron (one of the two spin-degenerate $CB_1$ transition can completely saturate due to state filling), the electron at $CB_{2,3(2),4}$ cannot transfer into the core state $CB_1$ because of the Coulomb blockade effect.[9] When $\langle N_0 \rangle$ = 3.1, the fast decay component disappears, indicating that the core state is completely occupied. Generally the decay lifetime of CdSe quantum dots is found to decrease with increasing the pump fluence because of the Auger recombination of multiple excitons in QDs.[23] Because of the near degeneracy of $CB_2$, $CB_{3(2)}$, and $CB_4$, it becomes possible to arrange one electron at one arm and another electron at another arm, which reduces the Auger recombination in tetrapod NCs.[22]

As shown in Figure 2c, the buildup time of bleaching signal at 640 nm is determined to be 0.86 ps, corresponding to an electron transfer process from arms to the core. The rise time is found to decrease from 0.86 to 0.37 ps with increasing the pump fluence, indicating direct relaxation from higher excited states to the lowest electron state $CB_1$. At the low pump fluence, the decay lifetime of $CB_1$ is about several nanoseconds, indicating that the core state is far away from the surface defect states. A fast decay process at the higher pump fluence is attributed to the Auger recombination.[23] When the average numbers of electron−hole pairs in a NC reach ⟨1.4⟩, ⟨3.1⟩, ⟨8.4⟩, ⟨14.8⟩, and ⟨23.9⟩, the decay times of the fast decay components are estimated to be about 208, 272, 65, 13, and 8 ps, respectively. For quantum dots with a diameter of 4.6 nm, the decay lifetimes of 1-, 2-, 3-, and 4-electron−hole pairs were 510, 45, 21, and 10 ps, respectively.[23] The Auger recombination rate in the tetrapod is slower than that in quantum dot, which is attributed to the electron in the tetrapod is extended into different areas, such as arms or core.[22,23] The fitted lifetimes of the core state $CB_1$ are summarized in Table S2 in Supporting Information. The decay lifetime of the higher state (probed at 493 nm) is found to increase with increasing pump fluence, indicating the relaxation time of hot electrons become long at the high pump fluence, as seen in Supporting Information Figure S3. The fitted lifetimes of the B3 peak at 493 nm are summarized in Table S3 in Supporting Information.

Tetrapod-shaped NCs have been used in solar cells as absorber layer, due to excellent electron transport property in arms of tetrapod.[12−15] Methylene blue ($MB^+$) is a typical organic electron acceptor molecule for semiconductor quantum dots.[28−30] Ultrafast charge separation from the quantum dots to $MB^+$ is fast enough to extract multiple excitons before their Auger recombination.[28] To understand the charge separation from tetrapod-shaped NCs to $MB^+$ molecules, the femtosecond TA spectra with $MB^+$ molecules are shown in Figure 4. The lifetimes of the arm states $CB_{2,3(2),4}$ and the core state $CB_1$ are found to decrease dramatically with adsorption of $MB^+$ molecules, indicating electron transfer from CdSe tetrapods to $MB^+$ molecules. The charge separation (CS) efficiency can


DOI: 10.1021/am5091148
ACS Appl. Mater. Interfaces 2015, 7, 7938−7944

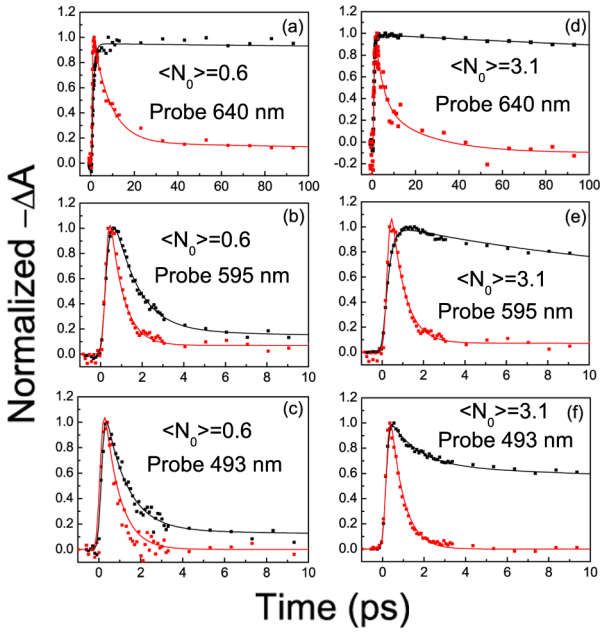


**Figure 4.** Normalized bleach signal kinetics of CdSe tetrapods without (black lines) and with (red lines) $MB^+$ molecules. $\langle N_0 \rangle$ are 0.6 (a, b, c) and 3.1 (d, e, f), respectively. Probe wavelengths are 640 (a, d), 595 (b, e), and 493 nm (c, f), respectively.

be calculated by $\eta_{CS} = 1 - \tau_{1/2(TP-MB^+)}/\tau_{1/2(TP)}$, where $\tau_{1/2(TP-MB^+)}$ and $\tau_{1/2(TP)}$ are half-life times for tetrapods with and without $MB^+$ molecules. The fitted lifetimes and charge separation efficiencies of tetrapod-shaped NCs with and without $MB^+$ molecules are summarized in Table 1. At low pump fluence ($\langle N_0 \rangle = 0.6$), the half-life times of the arm states $CB_{2,3(2),4}$ and the core state $CB_1$ for tetrapod-shaped NCs with $MB^+$ molecules are determined to be 0.62 and 6.91 ps, respectively. The corresponding charge separation efficiencies are 26% and 100%, respectively. Because the electron transfer process from arm states to the core state is also fast with a time constant of 1.04 ps, only a small part (26%) of electron in the arms transfers into $MB^+$ molecules. Before adsorption of $MB^+$ molecules on the arms, the maximum absorption change at 640 nm is 7.2 mOD. After adsorption of $MB^+$ molecules, the value becomes 2.1 mOD, indicating the charge separation from the arm states to $MB^+$ molecules before relaxation into the core state. At high pump fluence ($\langle N_0 \rangle = 3.1$), the half-life times of the arm states $CB_{2,3(2),4}$ and the core state $CB_1$ for tetrapods with $MB^+$ molecules are 0.47 and 3.73 ps, respectively. The corresponding charge separation efficiencies are 99% and 100%, respectively. This indicates that the efficient charge separation from arms of tetrapod to $MB^+$ molecules at the high pump fluence, due to the reduced electron relaxation process from the arm states to the core state. The decay time of electron at the higher state (probed at 493 nm) is found to increase with increasing pump fluence, possibly due to the Coulomb blockade of multiple electrons in one tetrapod.[9] The hot electron extraction from tetrapods to $MB^+$ molecules at the high pump fluence ($\eta_{CS}$ = 82%) is more effective than that at the low pump fluence ($\eta_{CS}$ = 60%), as shown in Figure 5. The experimental result indicates that the hot electrons can be easily extracted from tetrapod-shaped NCs, showing a potential application in photovoltaic devices.

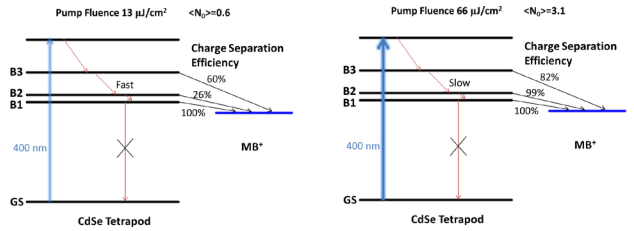


**Figure 5.** Schematic diagram of charge separation processes from different energy levels of CdSe tetrapod to $MB^+$ molecule under low (left) and high (right) pump fluences. B1, B2, and B3 are the assigned absorption bands in Figure 2b. GS is the ground state. Blue solid arrows, red dot arrows, red solid arrows, and black solid arrows represent excitation, relaxation, radiative recombination, and charge separation processes, respectively.

## 4. CONCLUSION

In conclusion, we have studied the ultrafast carrier dynamics and hot electron extraction in tetrapod-shaped CdSe NCs by femtosecond TA spectroscopy. The lowest electronic state $CB_1$ localized in the core exhibited a rapid rise time of 0.86 ps and long decay time of 5 ns, which is important for the device applications of the single tetrapod transistor. The state filling mechanism of CdSe tetrapods was revealed under various pump fluence. At the low pump fluence, the carriers relax from

**Table 1. Summary of Biexponential Fit Parameters for Kinetics of CdSe Tetrapod NCs without or with $MB^+$ Molecules and the Calculated Charge Separation Efficiencies for Different Energy States Shown in Figure 4**

| $\langle N_0 \rangle$ | probe wavelength (nm) | with $MB^+$ (yes or no) | $\tau_{Raise}$ (ps) | $A_{Decay1}$ (%) | $\tau_{Decay1}$ (ps) | $A_{Decay2}$ (%) | $\tau_{Decay2}$ (ps) | $\tau_{1/2}{}^a$ (ps) | $\eta_{CS}$ (%) |
|---|---|---|---|---|---|---|---|---|---|
| 0.6 | 640 | no | 0.86 | | | 100 | 5066.78 | 3817.01 | 100 |
| | | yes | 0.25 | 85 | 7.84 | 15 | 448.54 | 6.91 | |
| | 595 | no | 0.22 | 90 | 1.04 | 10 | 55.14 | 0.84 | 26 |
| | | yes | 0.04 | 90 | 0.76 | 10 | 1725.87 | 0.62 | |
| | 493 | no | 0.03 | 88 | 0.99 | 12 | 50.68 | 0.83 | 60 |
| | | yes | 0.03 | 100 | 0.48 | | | 0.33 | |
| 3.1 | 640 | no | 0.42 | 26 | 272.49 | 74 | 4404.71 | 1730.83 | 100 |
| | | yes | 0.37 | 61 | 3.55 | 39 | 12.25 | 3.74 | |
| | 595 | no | 0.25 | 39 | 11.25 | 61 | 196.05 | 42.51 | 99 |
| | | yes | 0.04 | 96 | 0.64 | 4 | 289.27 | 0.47 | |
| | 493 | no | 0.04 | 58. | 1.22 | 42 | 106.51 | 2.29 | 82 |
| | | yes | 0.02 | 100 | 0.60 | | | 0.42 | |

[a]The half-life time, $\tau_{1/2}$, is defined as $A_{Decay1}e^{-((\tau_{1/2})/(\tau_{Decay1}))} + A_{Decay2}e^{-((\tau_{1/2})/(\tau_{Decay2}))} = 1/2$.



DOI: 10.1021/am5091148
ACS Appl. Mater. Interfaces 2015, 7, 7938−7944

the higher electronic states ($CB_2$, $CB_{3(2)}$, and $CB_4$) to the lowest electronic state $CB_1$ at time constant of 1.04 ps. Coulomb blockade effect was observed in carrier dynamics of tetrapods at the high pump fluence. The hot electrons at the arm states could be extracted by the adsorbed electron acceptor molecules, especially under excitation at the high pump fluence. The ultrafast carrier dynamics in tetrapod-shaped NCs obtained from this work highlights the importance of morphology controllable electronic structure.

## ■ ASSOCIATED CONTENT

### Supporting Information

TEM images of tetrapod-shaped CdSe NCs, steady state versus transient absorption spectra with high pump fluence, normalized bleach signal kinetics are probed at 493 nm with different pump fluences, and summary of multiexponential fit parameters for kinetics probed at 640, 595, and 493 nm. This material is available free of charge via the Internet at http://pubs.acs.org.

## ■ AUTHOR INFORMATION


### Corresponding Authors

*Phone: +86-431-86176030. E-mail: jiwy@ciomp.ac.cn.
*Phone: +86-431-86176313. E-mail: zhaojl@ciomp.ac.cn.


### Notes

The authors declare no competing financial interest.

## ■ ACKNOWLEDGMENTS

This work was supported by the National Natural Science Foundation of China (Nos. 11204298, 61205025, 11274304, and 61274126), Jilin Province Science and Technology Research Project (Nos. 20140101060JC, 20150519003JH), and the Innovative Research Support Program (Pilot Model) of University of Tsukuba, Japan.

## ■ REFERENCES


(1) Manna, L.; Scher, E. C.; Alivisatos, A. P. Synthesis of Soluble and Processable Rod-, Arrow-, Teardrop-, and Tetrapod-Shaped CdSe Nanocrystals. *J. Am. Chem. Soc.* **2000**, *122*, 12700−12706.

(2) Manna, L.; Milliron, D. J.; Meisel, A.; Scher, E. C.; Alivisatos, A. P. Controlled Growth of Tetrapod-Branched Inorganic Nanocrystals. *Nat. Mater.* **2003**, *2*, 382−385.

(3) Chen, S. H.; Wang, Z. L.; Ballato, J.; Foulger, S. H.; Carroll, D. L. Monopod, Mipod, Tripod, and Tetrapod Gold Nanocrystals. *J. Am. Chem. Soc.* **2003**, *125*, 16186−16187.

(4) Li, Y. C.; Zhong, H. Z.; Li, R.; Zhou, Y.; Yang, C. H.; Li, Y. F. High-Yield Fabrication and Electrochemical Characterization of Tetrapodal CdSe, CdTe, and $CdSe_xTe_{1-x}$ Nanocrystals. *Adv. Funct. Mater.* **2006**, *16*, 1705−1716.

(5) Fiore, A.; Mastria, R.; Lupo, M. G.; Lanzani, G.; Giannini, C.; Carlino, E.; Morello, G.; De Giorgi, M.; Li, Y.; Cingolani, R.; Manna, L. Tetrapod-Shaped Colloidal Nanocrystals of II-VI Semiconductors Prepared by Seeded Growth. *J. Am. Chem. Soc.* **2009**, *131*, 2274−2282.

(6) Xie, R. G.; Kolb, U.; Basche, T. Design and Synthesis of Colloidal Nanocrystal Heterostructures with Tetrapod Morphology. *Small* **2006**, *2*, 1454−1457.

(7) Li, J. B.; Wang, L. W. Shape Effects on Electronic States of Nanocrystals. *Nano Lett.* **2003**, *3*, 1357−1363.

(8) Choi, C. L.; Alivisatos, A. P. From Artificial Atoms to Nanocrystal Molecules: Preparation and Properties of More Complex Nanostructures. *Annu. Rev. Phys. Chem.* **2010**, *61*, 369−389.

(9) Cui, Y.; Banin, U.; Björk, M. T.; Alivisatos, A. P. Electrical Transport through a Single Nanoscale Semiconductor Branch Point. *Nano Lett.* **2005**, *5*, 1519−1523.

(10) Schrier, J.; Lee, B.; Wang, L. W. Mechanical and Electronic-Structure Properties of Compressed CdSe Tetrapod Nanocrystals. *J. Nanosci. Nanotechnol.* **2008**, *8*, 1994−1998.

(11) Choi, C. L.; Koski, K. J.; Sivasankar, S.; Alivisatos, A. P. Strain-Dependent Photoluminescence Behavior of CdSe/CdS Nanocrystals with Spherical, Linear, and Branched Topologies. *Nano Lett.* **2009**, *9*, 3544−3549.

(12) Sun, B.; Marx, E.; Greenham, N. C. Photovoltaic Devices Using Blends of Branched CdSe Nanoparticles and Conjugated Polymers. *Nano Lett.* **2003**, *3*, 961−963.

(13) Dayal, S.; Reese, M. O.; Ferguson, A. J.; Ginley, D. S.; Rumbles, G.; Kopidakis, N. The Effect of Nanoparticle Shape on the Photocarrier Dynamics and Photovoltaic Device Performance of Poly(3-hexylthiophene):CdSe Nanoparticle Bulk Heterojunction Solar Cells. *Adv. Funct. Mater.* **2010**, *20*, 2629−2635.

(14) Dayal, S.; Kopidakis, N.; Olson, D. C.; Ginley, D. S.; Rumbles, G. Photovoltaic Devices with a Low Band Gap Polymer and CdSe Nanostructures Exceeding 3% Efficiency. *Nano Lett.* **2010**, *10*, 239−242.

(15) Crisp, R. W.; Panthani, M. G.; Rance, W. L.; Duenow, J. N.; Parilla, P. A.; Callahan, R.; Dabney, M. S.; Berry, J. J.; Talapin, D. V.; Luther, J. M. Nanocrystal Grain Growth and Device Architectures for High-Efficiency CdTe Ink-Based Photovoltaics. *ACS Nano* **2014**, *8*, 9063−9072.

(16) Choi, C. L.; Li, H.; Olson, A. C. K.; Jain, P. K.; Sivasankar, S.; Alivisatos, A. P. Spatially Indirect Emission in a Luminescent Nanocrystal Molecule. *Nano Lett.* **2011**, *11*, 2358−2362.

(17) Wong, J. I.; Mishra, N.; Xing, G.; Li, M.; Chakrabortty, S.; Sum, T. C.; Shi, Y.; Chan, Y.; Yang, H. Y. Dual Wavelength Electroluminescence from CdSe/CdS Tetrapods. *ACS Nano* **2014**, *8*, 2873−2879.

(18) Liu, Su.; Borys, N. J.; Huang, J.; Talapin, D. V.; Lupton, J. M. Exciton Storage in CdSe/CdS Tetrapod Semiconductor Nanocrystals: Electric Field Effects on Exciton and Multiexciton States. *Phys. Rev. B* **2012**, *86*, No. 045303.

(19) Malkmus, S.; Kudera, S.; Manna, L.; Parak, W. J.; Markus, B. Electron-Hole Dynamics in CdTe Tetrapods. *J. Phys. Chem. B* **2006**, *110*, 17334−17338.

(20) Peng, P.; Milliron, D. J.; Hughes, S. M.; Johnson, J. C.; Alivisatos, A. P.; Saykally, R. J. Femtosecond Spectroscopy of Carrier Relaxation Dynamics in Type II CdSe/CdTe Tetrapod Heteronanostructures. *Nano Lett.* **2005**, *5*, 1809−1813.

(21) Mauser, C.; Da Como, E.; Baldauf, J.; Rogach, A. L.; Huang, J.; Talapin, D. V.; Feldmann, J. Spatio-Temporal Dynamics of Coupled Electrons and Holes in Nanosize CdSe-CdS Semiconductor Tetrapods. *Phys. Rev. B* **2010**, *82*, No. 081306.

(22) Wang, L. W. Charging Effects in a CdSe Nanotetrapod. *J. Phys. Chem. B* **2005**, *109*, 23330−23335.

(23) Klimov, V. I.; Mikhailovsky, A. A.; McBranch, D. W.; Leatherdale, C. A.; Bawendi, M. G. Quantization of Multiparticle Auger Rates in Semiconductor Quantum Dots. *Science* **2000**, *287*, 1011−1013.

(24) Klimov, V. I.; McBranch, D. W.; Leatherdale, C. A.; Bawendi, M. G. Electron and Hole Relaxation Pathways in Semiconductor Quantum Dots. *Phys. Rev. B* **1999**, *60*, 13740−13749.

(25) Matylitsky, V. V.; Dworak, L.; Breus, V. V.; Basché, T.; Wachtveitl, J. Ultrafast Charge Separation in Multiexcited CdSe Quantum Dots Mediated by Adsorbed Electron Acceptors. *J. Am. Chem. Soc.* **2009**, *131*, 2424−2425.

(26) Trinh, M. T.; Houtepen, A. J.; Schins, J. M.; Hanrath, T.; Piris, J.; Knulst, W.; Goossens, A.; Siebbeles, L. D. A. In Spite of Recent Doubts Carrier Multiplication Does Occur in PbSe Nanocrystals. *Nano Lett.* **2008**, *8*, 1713−1718.

(27) Klimov, V. I. Optical Nonlinearities and Ultrafast Carrier Dynamics in Semiconductor Nanocrystals. *J. Phys. Chem. B* **2000**, *104*, 6112−6123.

(28) Yang, Y.; Rodríguez-Córdoba, W.; Lian, T. Ultrafast Charge Separation and Recombination Dynamics in Lead Sulfide Quantum




DOI: 10.1021/am5091148
ACS Appl. Mater. Interfaces 2015, 7, 7938−7944

Dot−Methylene Blue Complexes Probed by Electron and Hole Intraband Transitions. *J. Am. Chem. Soc.* **2011**, *133*, 9246−9249.
(29) Huang, J.; Huang, Z.; Yang, Y.; Zhu, H.; Lian, T. Multiple Exciton Dissociation in CdSe Quantum Dots by Ultrafast Electron Transfer to Adsorbed Methylene Blue. *J. Am. Chem. Soc.* **2010**, *132*, 4858−4864.
(30) Jing, P. T.; Ji, W. Y.; Yuan, X.; Ikezawa, M.; Zhang, L. G.; Li, H. B.; Zhao, J. L.; Masumoto, Y. Photoinduced Charge Separation and Recombination Processes in CdSe Quantum Dot and Graphene Oxide Composites with Methylene Blue as Linker. *J. Phys. Chem. Lett.* **2013**, *4*, 2919−2925.



DOI: 10.1021/am5091148
*ACS Appl. Mater. Interfaces* 2015, 7, 7938−7944